



| | |
|------------------|--|
| Title | Bioimaging of Pb and STIM1 in mice liver, kidney and brain using Laser Ablation Inductively Coupled Plasma Mass Spectrometry (LA-ICP-MS) and immunohistochemistry |
| Author(s) | Togao, Masao; Nakayama, Shouta M. M.; Ikenaka, Yoshinori et al. |
| Citation | Chemosphere, 238, 124581 https://doi.org/10.1016/j.chemosphere.2019.124581 |
| Issue Date | 2020-01-01 |
| Doc URL | https://hdl.handle.net/2115/83751 |
| Rights | © 2020. This manuscript version is made available under the CC-BY-NC-ND 4.0 license https://creativecommons.org/licenses/by-nc-nd/4.0/ |
| Rights(URL) | https://creativecommons.org/licenses/by-nc-nd/4.0/ |
| Type | journal article |
| File Information | Manuscript.pdf |



Title

Bioimaging of Pb and STIM1 in mice liver, kidney and brain using Laser Ablation Inductively Coupled Plasma Mass Spectrometry (LA-ICP-MS) and immunohistochemistry

Short title

Bioimaging of Pb and STIM1 in mice liver, kidney and brain

Author names

Masao Togao ^{1, a)}, Shouta M.M. Nakayama ^{1, a)}, Yoshinori Ikenaka ^{1, 2)}, Hazuki Mizukawa ³⁾, Yoshiki Makino ⁴⁾, Ayano Kubota ⁵⁾, Takehisa Matsukawa ⁵⁾, Kazuhito Yokoyama ⁵⁾, Takafumi Hirata ⁶⁾, Mayumi Ishizuka ^{1, *)}

Authors' affiliation

(1) Laboratory of Toxicology, Department of Environmental Veterinary Sciences, Graduate School of Veterinary Medicine, Hokkaido University, Kita 18 Nishi 9, Kita-ku, Sapporo 060-0818, Japan

(2) Water Research Group, School of Environmental Sciences and development, North-West University, South Africa

(3) Department of Science and Technology for Biological Resources and Environment, Graduate School of Agriculture, Ehime University, Tarumi 3-5-7, Matsuyama, Ehime, 790-8566 Japan

(4) Division of Earth and Planetary Sciences, Kyoto University, Kyoto, Japan

(5) Department of Epidemiology and Environmental Health, Juntendo University Faculty of Medicine, Tokyo, Japan

(6) Graduate School of Science, The University of Tokyo, Tokyo, Japan

(a) Both authors equally contributed to this study (Dual first authorship).

Authors' e-mail address:

Masao Togao <togamasa12@gmail.com>

Shouta M.M. Nakayama <shouta-nakayama@vetmed.hokudai.ac.jp>

Yoshinori Ikenaka <y_ikenaka@vetmed.hokudai.ac.jp>

Hazuki Mizukawa <hazuki.mizukawa@vetmed.hokudai.ac.jp>

Yoshiki Makino <y.makino.kueps@gmail.com>

Ayano Kubota <ay-kubota@juntendo.ac.jp>

Takehisa Matsukawa <tmatsuka@juntendo.ac.jp>
Kazuhito Yokoyama <kyokoya@juntendo.ac.jp>
Takafumi Hirata <hrt1@eqchem.s.u-tokyo.ac.jp>
Mayumi Ishizuka <ishizum@vetmed.hokudai.ac.jp>

***Corresponding author:**

Mayumi ISHIZUKA

E-mail: ishizum@vetmed.hokudai.ac.jp

Laboratory of Toxicology, Department of Environmental Veterinary Sciences, Graduate School of Veterinary Medicine, Hokkaido University, N18, W9, Kita-ku, Sapporo 060-0818, Japan

Tel: +81-11-706-6949; Fax: +81-11-706-510

1 **Abstract**

2 Lead (Pb) pollution is one of the most serious environmental problems and has
3 attracted worldwide attention. Pb causes hematological, central nervous system, as well
4 as renal toxicity, and so on. Although many investigations about Pb in blood to evaluate
5 pollution status and toxic effects have been reported, there are open question about
6 biological behavior of Pb. In order to reveal any toxicological mechanisms or influences,
7 we focused on the local distribution of Pb in mice organs. Lead acetate (100 mg/L and
8 1,000 mg/L) in drinking water were given to the BALB/c mice (male, seven weeks of
9 age, N = 24) for three weeks. Laser Ablation Inductively Coupled Plasma Mass
10 Spectrometry (LA-ICP-MS) analysis revealed a homogenous distribution of Pb in the
11 liver and inhomogeneous distribution in the kidney and brain. The hippocampus,
12 thalamus, and hypothalamus had higher concentrations than other areas such as the
13 white matter. Surprisingly, in the kidney, Pb tended to accumulate in the medulla rather
14 than the cortex, strongly suggesting that high sensitivity areas and high accumulation
15 areas differ. Moreover, distribution of stromal interacting protein 1 which is candidate
16 gene of Pb pathway to the cells was homogenous in the liver and kidney whereas
17 inhomogeneous in the brain. In contrast to our hypothesis, interestingly, Pb exposure
18 under the current condition did not induce mRNA expressions for any candidate channel
19 or transporter genes. Thus, further study should be conducted to elucidate the local
20 distribution of Pb and other toxic metals, and pathway that Pb takes to the cells.

21

22 **Keywords**

23 Cell entry mechanisms

24 Laser Ablation Inductively Coupled Plasma Mass Spectrometry (LA-ICP-MS)

25 Distribution

26 Pb

27 Stromal interacting protein 1 (STIM1)

28

29

30

31

32

33

34

35

36

37

38

39

40

41

42

43

44

45

46

47

48 **1. Introduction**

49 Elemental analysis of biological samples including internal organs are mainly
50 conducted by atomic absorption spectrometry (AAS; Yabe et al., 2012), Inductively
51 coupled plasma-atomic emission spectrometry (ICP-OES; Rahil-Khazen et al., 2002),
52 and inductively coupled plasma-mass spectrometry (ICP-MS; Nakata et al., 2016).
53 Usually, liquid samples are analyzed by such techniques, therefore organs are acid
54 digested and there is an assumption that they contain a homogeneous distribution of
55 investigated element (Konz et al., 2012). However, it is unknown about distribution
56 patterns of elements such as Pb, Cd and Hg in organs. If they are inhomogeneously
57 distributed, the evaluation of their concentrations in organs should be reconsidered.

58 Elemental analysis using ICP-MS combined with laser ablation (LA) has been
59 conducted (Pozebon et al., 2014, Noël et al., 2015, Yamashita et al., 2019). A solid
60 surface of sample is ablated by a pulse laser beam in the laser ablation chamber, the
61 ablated material is then analyzed by ICP-MS. Scanning of the surface by LA allows the
62 construction of images of elements distribution (Becker et al., 2010, Yamashita et al.,
63 2019). This method allows direct analysis of solid sample surfaces and is applicable for
64 thin organ slices (Becker et al., 2005, 2010, Ishii et al., 2018, Limbeck et al., 2015).
65 Numerous studies have used this method to analyze the local distribution of essential
66 elements such as Cu, Fe, and Zn in organs, bones and teeth in human and animals
67 (Becker et al., 2015, Ishii et al., 2018, Johnston et al., 2019, Paul et al., 2015, Urgast et
68 al., 2012). However, with regards to Pb, there is still less published research which
69 investigate distribution in organs and bones (Dobrowolska et al., 2008, Ishii et al., 2018,
70 Johnston et al., 2019). Dobrowolska et al. (2008) showed a homogeneous Pb
71 distribution in brain regions. However, they analyzed the human brain (postmortem
72 from a healthy donor) and found very low Pb levels. Ishii et al. (2018) revealed the

73 distribution of Pb in bone of raptor species. To our best knowledge, there has not yet
74 been any research using Pb administrated laboratory animals (e.g. mice models) to
75 elucidate the local distribution of Pb in internal organs.

76 Despite various research efforts, the pathway by which Pb enters cells remains
77 unclear; this is still one of the important points concerning Pb toxicity (Chang et al.,
78 2008, Zhang et al., 2014). Pb^{2+} has the ability to mimic Ca^{2+} and other divalent metal
79 ions such as Fe^{2+} and Zn^{2+} (Zhang et al., 2014). Based on this mimicry, Ca^{2+} and other
80 divalent metal channels might be candidates for Pb entry (Godwin 2001). Two types of
81 Ca^{2+} channels: voltage gated Ca^{2+} channels (VGCCs) and store operated Ca^{2+} channels
82 (SOCs), have been identified as potential routes by which Pb can enter cells (Kerper and
83 Hinkle 1997). With regards to VGCCs, this would only be feasible for excitable cells.
84 However, Pb may enter not only excitable cells but also other cells such as human
85 embryonic kidney cell 293 (Zhang et al., 2014, Chiu et al., 2009). Thus, VGCCs may
86 still provide a pathway to cells, but there must also be an additional route by which Pb
87 enters the cells in the rest of the body.

88 Some researchers have proposed that SOCs may play an important role in Pb
89 entry into cells (Chang et al., 2008, Kerper and Hinkle 1997, Chiu et al., 2009). SOCs
90 are constituted from transient receptor potentials (TRPs) and Orai1 present in the
91 plasma membrane, as well as from stromal interacting protein 1 (STIM1) present in the
92 endoplasmic reticulum (ER) membrane (Chang et al., 2008, Zhang et al., 2014, Chiu et
93 al., 2009).

94 Researchers have shown that STIM1 can translocate to interact with both Orai1
95 and TRPC1 during the activation of SOCs (Cheng et al., 2008, Liao et al., 2008).
96 Although some research has indicated that STIM1 may be a key protein by which Pb

97 enters the cell (Chang et al., 2008, Chiu et al., 2009), and may contribute to the
98 localization of STIM1 (Klejman et al., 2009, Skibinska-Kijek et al., 2009), no studies
99 have compared local distribution of Pb with that of STIM1. Additionally, to our
100 knowledge, no studies have yet confirmed whether Pb induces STIM1.

101 In view of the above, we conducted an experiment using mice to achieve the
102 following aims: (1) to demonstrate the local distribution of Pb in organs; (2) to compare
103 the distribution of STIM1 with that of Pb; and (3) to clarify whether Pb induces STIM1.

104

105 **2. Materials and methods**

106 **2.1. Animals**

107 BALB/c mice (male, seven weeks of age, N = 24) were purchased from Sankyo
108 Labo Service Corporation, Inc. (Tokyo, Japan). The mice were divided into three groups
109 and housed in six polypropylene cages (N = 4 per batch). One batch from each group
110 (control, low, and high) was sampled for ICP-MS, and the other batch from each group
111 for LA-ICP-MS. There was no significant difference in body weight between groups
112 (supplementary Figure S1). The animals were allowed to acclimate to the animal
113 facilities at the Graduate School of Veterinary Medicine, Hokkaido University for one
114 week prior to testing. Under these conditions, food (rodent chow, Labo MR Stock,
115 Nosan Corporation, Yokohama, Japan) and distilled water were provided *ad libitum*.
116 After acclimation, two different concentrations of lead acetate: 100 mg/L and 1,000
117 mg/L (Wako Pure Chemical Industries, Osaka, Japan) were given to two of the groups
118 (the low and high dosage groups, respectively) in the drinking water for three more
119 weeks. In our preliminary experiment, dose dependent increase of Pb concentration in
120 blood and organs were observed when we selected 100 mg/L and 1,000 mg/L for three
121 weeks of exposure (data not shown). The control groups were provided with distilled
122 water. After three weeks of exposure, mice were anesthetized with sevoflurane and
123 blood and organs (liver, kidney, and brain) were collected via the following methods.
124 For the ICP-MS groups, blood and organ samples were collected in polypropylene tubes,
125 then stored at -80°C in a deep freezer. For the LA-ICP-MS groups, organ samples were
126 embedded in Tissue-Tec OCT (Sakura Finetek, CA, USA), quickly frozen in isopentane
127 which had been cooled with dry ice, then stored at -80°C in a deep freezer. Additionally,
128 small pieces of the liver, kidney, and brain samples were collected together with

129 RNAlater Tissue Storage and RNA Stabilization Solution (Sigma-Aldrich, MO, USA)
130 in polypropylene tubes and stored at -80°C in a deep freezer for real time PCR and
131 microarray analysis. All experiments using animals were performed under the
132 supervision and with the approval of the Institutional Animal Care and Use Committee
133 of Hokkaido University, Japan (approval number: 16-0017, approval day: 29th March
134 2016).

135

136 **2.2. Quantitative analysis by ICP-MS**

137 The ICP-MS groups were used for the quantitative analysis of Pb concentration.
138 In this case, blood, liver, kidney, and brain were acid digested using the method
139 described by Nakata et al. (2016, 2015) with minor modifications. The whole kidney,
140 liver, and brain samples were dried for 48 hours in an oven at 50°C. Then, 0.1 mL of the
141 blood samples and approximately 0.1 g of the dried biological samples were weighted
142 and placed in pre-washed digestion vessels. This was followed by acid digestion using 5
143 mL of nitric acid (atomic absorption spectrometry grade, 30%; Kanto Chemical, Tokyo,
144 Japan), and 1 mL of hydrogen peroxide (Cica reagent, 30%; Kanto Chemical). The
145 digestion vessels subsequently underwent a ramped temperature program in a closed
146 microwave system (Speed Wave MWS-2 microwave digestion system; Berghof,
147 Eningen, Germany). The operating conditions of microwave system are given in the
148 supplementary Table S1. After cooling, the sample solutions were transferred into 15
149 mL polypropylene tubes and diluted to a final volume of 10 mL with bi-distilled and
150 de-ionized water (Milli-Q).

151 The Pb concentrations determination was performed using the procedure
152 described by Nakata et al. (2016, 2015) with minor modifications. Concentration of Pb

153 was measured by ICP-MS (7700 series; Agilent Technologies, Tokyo, Japan). The
154 operating conditions of ICP-MS are given in the supplementary Table S2. Quality
155 control was conducted by analysis of DORM-3 (fish protein; National Research Council
156 of Canada, Ottawa, Canada) and DOLT-4 (dogfish liver; National Research Council of
157 Canada) certified reference materials. Replicate analysis of these reference materials
158 showed good recovery rates (95–105%); the instrument detection limit for Pb was 0.001
159 $\mu\text{g/L}$.

160

161 **2.3. Analysis by LA-ICP-MS**

162 Sections of embedded liver, kidney, and brain were cut on a cryostat to a
163 thickness of 20 μm . The native cryosections were then mounted directly onto glass
164 slides. Then, they were analyzed using an LA system (NWR213; esi Japan, Tokyo,
165 Japan) associated with an ICP-MS instrument (8800 series; Agilent Technologies,
166 Tokyo, Japan). The tissue sections were systematically scanned by a focused laser beam
167 (line by line: spot size 100 μm , scan speed 100 $\mu\text{m}/\text{sec}$, scan step 100 μm). Measured
168 isotope (dwell time, sec) were as follows; ^{13}C (0.005), ^{25}Mg (0.005), ^{31}P (0.005), ^{43}Ca
169 (0.005), ^{55}Mn (0.005), ^{57}Fe (0.005), ^{65}Cu (0.005), ^{66}Zn (0.005), ^{206}Pb (0.01), ^{207}Pb (0.01),
170 ^{208}Pb (0.01). In this analysis, no quantification of Pb was conducted due to lack of
171 suitable reference materials for calibration, however intensity of Pb (and other elements)
172 was normalized to ^{13}C (carbon) intensity as Wu et al. (2009), Johnston et al. (2019) and
173 others have utilized to normalize the ablation efficiency. Detailed analytical conditions
174 are presented in supplementary Table S3. From the continuous list of raw pixel values
175 data, elemental images were reconstructed using LA-ICP-MS Image generator
176 house-made software iQquant2 (Kawakami et al., 2016).

177

178 **2.4. Immunohistochemistry**

179 Immunohistochemistry (IHC) was carried out using the method described by
180 Skibinska-Kijek et al. (2009) and Wang et al. (2010) with minor modifications. Sections
181 of the embedded liver, kidney, and brain samples were cut on a cryostat to a thickness of
182 20 μm . After fixation with 4% paraformaldehyde phosphate buffer solution and
183 quenching of endogenous peroxidase activity with 0.3% H_2O_2 in methanol, the sections
184 were blocked with goat serum in Phosphate Buffered Saline (PBS). Then, the sections
185 were incubated overnight at 4°C with antibody recognizing STIM1 (ProteinTech Group
186 Inc., cat no 11565-1-AP, the antibody was raised against an N-terminal fragment of the
187 protein: aa 2-350) diluted 1:200 in PBS. Samples were then washed and incubated with
188 biotinylated secondary antibodies (Vector Laboratories, Burlingame, CA, USA) in PBS
189 for thirty minutes. After washing, the sections were incubated with Avidin-biotin
190 complex reagent (ABC-Elite kit, Vector Laboratories), following the manufacturers
191 protocol. The immunocomplex was visualized with diaminobenzidine (DAB) (Vector
192 Laboratories), sections were counterstained with haematoxylin (Sigma-Aldrich), and
193 observations were conducted by microscope (BIOREVO BZ-9000 series; KEYENCE,
194 Osaka, Japan).

195

196 **2.5. Quantitative analysis by real time PCR**

197 Real time PCR was performed using the method described by Skibinska-Kijec
198 et al. (2009) with small modifications. Total RNA was extracted from small pieces of
199 liver, kidney, and brain soaked in RNAlater (Sigma-Aldrich) using Nucleo spin (Takara
200 bio, Shiga, Japan). First-strand cDNA was generated from 600 ng of total RNA in a

201 final volume of 20 μ L with ReverTra Ace (Toyobo, Osaka, Japan). This was examined
202 by real time PCR with specific gene primers for *Stim1* (NM_009287;
203 (5'GCTCTCAATGCCATGCCTTCCAAT, 5'TCTAGGCCATGGTTCAACGCCATA),
204 and Fast SYBR Green Master mix (Applied Biosystems). The samples were analyzed
205 using 7000 Sequence Detection System hardware and software (Applied Biosystems).
206 *18S ribosomal RNA* (NR_003278) for normalization was used with the following
207 primers: 5'AACGAACGAGACTCTGGCATG and
208 5'CGGACATCTAAGGGCATCACA. A relative quantification (RQ) method was used
209 to calculate the relative levels of *Stim1* mRNA. The formula was as follows: $RQ =$
210 $2^{-\Delta\Delta CT}$, where $\Delta\Delta CT = CT(\text{target}) - CT(18S)$. Amplification efficiency was 98.0% for
211 *STIM1* and 100.5% for *18S ribosomal RNA*.

212

213 **2.6. Microarray analysis**

214 To analyze gene expression profiles, a microarray experiment was performed.
215 Firstly, the total RNA of the liver, kidney, and brain was quantified and qualified using
216 an Agilent 2100 Bioanalyzer series II (Agilent Technologies, supplementary Table S4).
217 Cyanine 3-labelled cRNA was prepared from 500 ng of total RNA, and amplified using
218 a Low Input Quick Amp Labeling Kit (Agilent Technologies), according to the
219 manufacturer's instructions, followed by RNeasy column purification (Qiagen,
220 Valencia, CA). Dye incorporation and cRNA yield were checked with the NanoDrop
221 ND-1000 Spectrophotometer the Agilent 2100 Bioanalyzer. Gene Expression (GE)
222 Hybridization Kit (Agilent Technologies) was used for labeling. 600 ng of Cy3-labelled
223 cRNA was fragmented at 60°C for 30 minutes following the manufacturer's instructions.
224 On completion of the fragmentation reaction, 25 μ L of 2x Agilent hybridization buffer

225 was added to the fragmentation mixture and hybridized to Agilent SurePrint G3 Mouse
226 8 x 60K ver.2.0 for 17 hours at 65°C in a rotating Agilent hybridization oven. After
227 hybridization, slides were washed 1 minute at room temperature with GE Wash Buffer 1
228 (Agilent) and 1 minute with 37°C GE Wash buffer 2 (Agilent), then air-dried
229 immediately. Slide was scanned immediately after washing on the Agilent DNA
230 Microarray Scanner using one color scan setting (Agilent Technologies, Scan
231 Resolution; 3 µm, TIFF file dynamic range; 20bit). The scanned images were analyzed
232 with Feature Extraction Software 12.0.3.1 (Agilent) using default parameters to obtain
233 background subtracted and spatially detrended Processed Signal intensities. Normalized
234 (75 Percentile Shift) signal intensity was used for data acquisition. The data for
235 microarray is deposited at the NCBI Gene Expression Omnibus (GEO) database;
236 accession number is “Series GSE93544”.

237

238 **2.7. Statistical analysis**

239 All statistical analyses were carried out using JMP 12 (SAS Institute, Cary, NC,
240 USA). A Tukey-Kramer test was performed to compare body weights, Pb concentration,
241 and gene expression of STIM1 in tissue samples between groups. All statistical analyses
242 were performed at a significance level of 95%.

243

244 **3. Results**

245 **3.1. Pb concentrations in mice organs**

246 Table 1 shows the mean \pm standard deviations (SD) of the Pb concentration in
247 the blood, liver, kidney, and brain of the three groups. A dose dependent increase of Pb
248 concentration in the organs was observed and there were significant differences in Pb
249 concentration in the blood and all tissue-types between the control and high Pb dosage
250 groups.

251

252 **3.2. Pb local distributions in mice organs**

253 The local distribution of Pb in the liver, kidney, and brain of the three mice
254 groups are shown in Figures 1, 2, and 3, respectively. A homogeneous distribution of Pb
255 was found in the liver of the low and high dosage groups (Figure 1). Yet surprisingly,
256 inhomogeneous Pb distribution was discovered in the kidney and brain (Figures 2 and
257 3). Within the kidney, in the internal area surrounding the medulla there was a higher
258 regional Pb concentration than in the renal cortex in the low and high dosage groups
259 (Figure 2). The brain also showed an inhomogeneous distribution; the hippocampus had
260 higher Pb concentration than other areas such as the white matter in high dosage group
261 (Figure 3). Pb in all tissues of the control group and in the brain of the low dosage group
262 was not detected as count values of ICP-MS were comparable to those of background
263 areas where only glass slide without organs (Figure 3). Additionally, other elements
264 distribution are shown in supplementary Figure S2. For example, Mn tended to
265 accumulate in the renal medulla than cortex (supplementary Figure S2 (D, E, F)), while
266 selective accumulation of Zn was observed in the hippocampus of brain (supplementary

267 Figure S2 (G, H, I)). These results were in accordance with the previous studies (Becker
268 et al., 2010, Shariatgorji et al., 2016).

269

270 **3.3. Immuno-localization of STIM1 in mice organs**

271 The reactivity of the primary antibody was confirmed by comparing it with
272 PBS (supplementary Figure S3). Figures 1, 2, and 3 show the immune-localization of
273 STIM1 in the liver, kidney, and brain of the three groups, respectively. A homogeneous
274 distribution of STIM1 was found in the liver and kidney in all groups (Figures 1 and 2).
275 However, the brain showed inhomogeneous distribution of STIM1: the gray matter and
276 hippocampus had higher densities than other areas such as the white matter in all groups
277 (Figure 3).

278

279 **3.4. Gene induction by Pb in mice organs**

280 Real time PCR was performed to measure the levels of STIM1 mRNA in the
281 liver, kidney, and brain. This confirmed that STIM1 was expressed in all organs (Figure
282 4). However, there were no significant differences in gene expression between groups in
283 any of the organs. Additionally, it was examined gene induction of the candidates
284 suspected to be responsible for Pb entry into cells such as STIM1, Orai1, TRP, VGCC,
285 divalent metal transporter 1, and anion exchanger in the liver, kidney, and brain by
286 microarray. However, no significant induction was observed in the liver, kidney, and
287 brain. As a confirmation, the induction of metallothionein, which is known to be
288 induced with Pb exposure, was observed to be two and eight times greater in the liver
289 and kidney, respectively, in the high dosage groups compared with the control group
290 (data not shown).

291 **4. Discussion**

292 **4.1. Pb local distribution in organs**

293 The local distribution of Pb and other toxic elements in organs is still unknown.
294 LA-ICP-MS allows direct analysis of thin organ sections (Becker et al., 2010). However,
295 as for Pb, there is little published research regarding bioimaging, especially in the Pb
296 exposed mice model.

297 In the present study, Pb concentration found in kidney (56.65 mg/kg) and liver
298 (16.49 mg/kg) in high dosage groups were comparable to that for lead-poisoned animals
299 in the previous study (Takano et al., 2015). By analysis using LA-ICP-MS, a
300 homogenous Pb distribution was found in the liver (Figure 1); however, the kidney and
301 brain showed inhomogeneous distribution of Pb (Figures 2 and 3) mainly in the kidney.
302 Since it was identified as a target soft tissue for Pb accumulation (Barregard et al.,
303 1999), there has been substantial research published on Pb concentration in animal
304 kidneys (Yabe et al., 2012, 2013, Bortey-Sam et al., 2015, Jarzynska et al., 2011,
305 Nakayama et al., 2011, 2013, Sedki et al., 2003). These reports were based on the
306 hypothesis that there is a homogenous distribution of Pb in the kidney, and thus did not
307 map the element in this organ. However, the present findings suggest that such mapping
308 should be considered for identifying toxic elements in the kidney. As Pb and other types
309 of toxic elements are mainly observed in the proximal tubule, which is primarily
310 distributed in the cortex, the proximal tubule was regarded to be the highest
311 accumulation area in the kidney (Sabolic 2006). Moreover, there are some reports about
312 studies focusing toxic elements distribution in the renal cortex (Smith et al., 1991, Wang
313 et al., 2009, Wlostowski et al., 2006), so, to some extent, it might be reasonable to focus
314 such region. A previous study using LA-ICP-MS to determine Pt in cisplatin

315 (Pt)-administrated rats found that Pt tended to accumulate in the cortex and
316 corticomedullary junction (Moreno-Gordaliza et al., 2011). However, the results of the
317 present study which revealed that Pb tended to accumulate in the medulla rather than the
318 cortex, strongly suggest that high sensitivity areas and high accumulation areas differ.
319 The present study would help to understand mechanism of pathological Pb toxicity.

320 Differences in Pb distribution among organs may be explained by their
321 individual characteristics. In histological anatomy and physiology, the liver is regarded
322 as a homogenous organ, thus Pb is distributed homogeneously. By contrast, the kidneys
323 and brain are regarded as inhomogeneous organs, therefore Pb is distributed
324 inhomogeneously.

325 In the present study, mice were selected to be the first proof of concept model,
326 yet the method utilized can be applied to other animals. For instance, previous research
327 has shown the tolerance of chickens to chronic Pb intoxication (Mazliah et al., 1989);
328 thus, revealing local distribution of Pb in chicken organs would be interesting.

329

330 **4.2. Comparison between Pb and STIM1 distribution and gene expression of** 331 **STIM1**

332 The present study found homogeneous distribution of STIM1, which is the
333 main component of SOCs, in the liver and kidney, whereas there was inhomogeneous
334 distribution in the brain (Figures 1, 2, and 3). There was a significant difference between
335 the distribution of Pb and STIM1 in the kidney which suggests that there are alternative
336 mechanisms underlying Pb distribution in the kidney. One explanation is that Pb
337 distribution is due to its reabsorption. In the kidney, Pb is filtered in the glomerulus;
338 however, most of this filtered Pb is reabsorbed by the distal tubule and the collecting

339 duct (Araki et al., 1983, 1978). The distal tubule and the collecting duct are primarily
340 located in the renal medulla, the area which had the highest concentration of Pb
341 compared with the other areas analyzed in the present study. As for channels and
342 transporters, the TRP super family, specifically TRP vanilloid (TRPV) 5, is responsible
343 for transcellular calcium (Ca^{2+}) reabsorption in the distal tubule, connecting tube, and
344 collecting duct of the kidney (Nijenhuis et al., 2005). Moreover, the Na^+ - Ca^{2+} exchanger
345 (NCX) and plasma membrane Ca^{2+} ATPase (PMCA) are responsible for the extrusion of
346 Ca^{2+} into the blood (Hoenderop et al., 2000). Despite the fact that there have not been
347 any studies revealing linkages between these transporters and Pb distribution, these
348 transporters might also be responsible for Pb^{2+} reabsorption and local distribution in the
349 kidney. Moreover, reabsorption behavior differs between Pb and other toxic metals such
350 as Cd, Hg (Araki et al., 1986); thus further study of transporters and other toxic
351 elements could be a key to support the idea proposed above.

352 In the brain, STIM1 is mainly distributed in the hippocampus, which is similar
353 with Pb distribution. Therefore, SOCs may be a candidate route for Pb entering brain
354 cells. However, VGCCs in the brain may also be a feasible candidate, as nerve cells are
355 excitable (Davila et al., 1999, Vassanelli and Fromherz 1998). Additionally, no
356 induction of STIM1 expression by Pb was observed in the current study, suggesting that
357 Pb enters the cells via other mechanisms.

358

359 **5. Conclusions**

360 In experimental animals such as mice model, local distribution of Pb was
361 demonstrated for liver, kidney and brain and compared with the distribution of Pb and
362 STIM1 for the first time. Inhomogeneous distribution of Pb was found in the kidney and

363 brain. In the kidney, Pb tended to accumulate in the medulla rather than the cortex. This
364 provides support for the mechanism of Pb toxicity as the proximal tubule is regarded as
365 an area of high accumulation. In this study, however, we did not find evidence
366 supporting that Pb enters the cells via SOCs. Thus, further study should be conducted to
367 elucidate the local distribution of Pb and other toxic elements, and pathway that Pb
368 takes to the cells.

369

370

371 **Acknowledgements**

372 The analyses were technically supported by Mr. Takahiro Ichise, Ms. Mio
373 Yagihashi and Ms. Nagisa Hirano. The English in this manuscript was proofread by
374 uni-edit (<https://uni-edit.net/usa>).

375 This work was supported by Grants-in-Aid for Scientific Research from the
376 Ministry of Education, Culture, Sports, Science and Technology of Japan awarded to M.
377 Ishizuka (No. 16H0177906, 18K1984708) and Y. Ikenaka (17K2003807, 18H0413208),
378 and S.M.M. Nakayama (No. 16K16197, 17KK0009), and the foundation of JSPS Core
379 to Core Program (AA Science Platforms), the Environment Research and Technology
380 Development Fund (SII-1/3-2, 4RF-1802/18949907) of the Environmental Restoration
381 and Conservation Agency of Japan. We also acknowledge financial support from The
382 Soroptimist Japan Foundation, The Nakajima Foundation, The Sumitomo foundation,
383 The Nihon Seimei Foundation and The Japan Prize Foundation. This research was also
384 supported by JST/JICA, SATREPS (Science and Technology Research Partnership for
385 Sustainable Development).

386

387 **Conflict of interest**

388 The authors declare no conflict of interest in this study.

389

390 **Author Contributions**

391 M.T., S.M.M.N., Y.M., Y.I., K.Y., T.H., and M.I. conceived and designed the
392 experiments; M.T., S.M.M.N., Y.M., A.K., and M.T. performed the experiments; M.T.,
393 S.M.M.N., and H.M. analyzed the data; M.T., S.M.M.N., Y.M. and M.I. have written the
394 manuscript; all authors have read and approved the final manuscript.

395

396 **Supplementary material**

397 Detailed information related to this study are available as supplementary material.

398

399

400

401

402

403

404

405

406

407

408

409

410

411 **Figure captions**

412 Figure 1. Distribution of ^{208}Pb and STIM1 in a 20 μm section of liver. Distribution of
413 $^{208}\text{Pb}/^{13}\text{C}$ analyzed by LA-ICP-MS (left). STIM1 was analyzed by IHC (right). Scale
414 bar is 3 mm. Among LA-ICP-MS images, the scale bar indicates the ratio of intensity
415 ($^{208}\text{Pb}/^{13}\text{C}$).

416

417 Figure 2. Distribution of ^{208}Pb and STIM1 in a 20 μm section of kidney. Distribution of
418 $^{208}\text{Pb}/^{13}\text{C}$ analyzed by LA-ICP-MS (left). STIM1 was analyzed by IHC (right). Scale
419 bar is 3 mm. Among LA-ICP-MS images, the scale bar indicates the ratio of intensity
420 ($^{208}\text{Pb}/^{13}\text{C}$).

421

422 Figure 3. Distribution of ^{208}Pb and STIM1 in a 20 μm section of brain. Distribution of
423 $^{208}\text{Pb}/^{13}\text{C}$ analyzed by LA-ICP-MS (left). STIM1 was analyzed by IHC (right). Scale
424 bar is 5 mm. Among LA-ICP-MS images, the scale bar indicates the ratio of intensity
425 ($^{208}\text{Pb}/^{13}\text{C}$).

426

427 Figure 4. Mean \pm SD of the expression of STIM1 in mice organs in the three dosage
428 groups: (A) liver, (B) kidney, and (C) brain. No significant differences were found
429 between groups.

430 **References**

431 Araki S. The effects of water restriction and water loading on urinary excretion of lead,
432 delta-aminolevulinic acid and coproporphyrin, *Br J Ind Med* 35 (1978) 312-317.

433

434 Araki S., Aono H., Yokoyama K., Murata K. Filterable plasma concentration,
435 glomerular filtration, tubular balance and renal clearance of heavy materials and organic
436 substances in metal workers, *Arch Environ Health* 41 (1986) 216-221.

437

438 Araki S., Murata K., Yokoyama K., Yanagihara S., Niinuma Y., Yamamoto R., Ishihara
439 N. Circadian rhythms in the urinary excretion of metals and organic substances in
440 'healthy' men, *Arch Environ Health* 38 (1983) 360-366.

441

442 Barregard L., Svalander C., Schutz A., Westberg G., Sallsten G., Blohme I., Molne J.,
443 Attman P.O., Haglind P. Cadmium, mercury, and lead in kidney cortex of the general
444 Swedish population: A study of biopsies from living kidney donors, *Environ. Health*
445 *Perspect.* 107 (1999) 867-871.

446

447 Becker J.S. Recent developments in isotope analysis by advanced mass spectrometric
448 techniques Plenary lecture, *J. Anal. At. Spectrom.* 20 (2005) 1173-1184.

449

450 Becker J.S., Breuer U., Hsieh H.F., Osterholt T., Kumtabtim U., Wu B., Matusch A.,
451 Caruso J.A., Qin Z.Y. Bioimaging of metals and biomolecules in mouse heart by laser
452 ablation inductively coupled plasma mass spectrometry and secondary ion mass
453 spectrometry, *Anal. Chem.* 82 (2015) 9528-9533.

454

455 Becker J.S., Zoriy M., Matusch A., Wu B., Salber D., Palm C. Bioimaging of metals by
456 laser ablation inductively coupled plasma mass spectrometry (LA-ICP-MS), *Mass*
457 *Spectrom. Rev.* 29 (2010) 156-175.

458

459 Bortey-Sam N., Nakayama S.M.M., Ikenaka Y., Akoto O., Baidoo E., Yohannes Y.B.,
460 Mizukawa H., Ishizuka M. Human health risks from metals and metalloid via
461 consumption of food animals near gold mines in Tarkwa, Ghana: Estimation of the daily
462 intakes and target hazard quotients (THQs), *Ecotoxicol. Environ. Saf.* 111 (2015)
463 160-167.

464

465 Chang Y. F., Teng H. C., Cheng S. Y., Wang C. T., Chiou S. H., Kao L. S., Kao F. J.,
466 Chiou A., Yang D.M. Orai1-STIM1 formed store-operated Ca²⁺ channels (SOCs) as the
467 molecular components needed for Pb²⁺ entry in living cells, *Toxicol. Appl. Pharmacol.*
468 227 (2008) 430-439.

469

470 Cheng K.T., Liu X.B., Ong H.L., Ambudkar I.S. Functional requirement for Orai1 in
471 store-operated TRPC1-STIM1 channels, *J. Biol. Chem.* 283 (2008) 12935-12940.

472

473 Chiu T.Y., Teng H.C., Huang P.C., Kao F.J., Yang D.M. Dominant role of Orai1 with
474 STIM1 on the cytosolic entry and cytotoxicity of lead ions, *Toxicol. Sci.* 110 (2009)
475 353-362.

476

477 Davila H.M. Molecular and functional diversity of voltage-gated calcium channels, Ann.
478 N. Y. Acad. Sci. 868 (1999) 102-117.
479

480 Dobrowolska J., Dehnhardt M., Matusch A., Zoriy M., Palomero-Gallagher N.,
481 Koscielniak P., Zilles K., Becker J.S. Quantitative imaging of zinc, copper and lead in
482 three distinct regions of the human brain by laser ablation inductively coupled plasma
483 mass spectrometry, Talanta 74 (2008) 717-723.
484

485 Godwin H.A. The biological chemistry of lead, Curr Opin Chem Biol 5 (2001) 223-227.
486

487 Hoenderop J.G.J., Hartog A., Stuiver M., Doucet A., Willems P., Bindels R.J.M.
488 Localization of the epithelial Ca²⁺ channel in rabbit kidney and intestine, J. Am. Soc.
489 Nephrol. 11 (2000) 1171-1178.
490

491 Ishii C., Nakayama S.M.M., Kataba A., Ikenaka Y., Saito K., Watanabe Y., Makino Y.,
492 Matsukawa T., Kubota A., Yokoyama K., Mizukawa H., Hirata T., Ishizuka M.
493 Characterization and imaging of lead distribution in bones of lead-exposed birds by
494 ICP-MS and LA-ICP-MS, Chemosphere 212 (2018) 994-1001.
495

496 Jarzynska G, Falandysz J. Selenium and 17 other largely essential and toxic metals in
497 muscle and organ meats of Red Deer (*Cervus elaphus*) - Consequences to human health,
498 Environ. Int. 37 (2011) 882-888.
499

500 Johnston, J.E., Franklin M., Roh H., Austin C., Arora. Lead and Arsenic in Shed
501 Deciduous Teeth of Children Living Near a Lead-Acid Battery Smelter. *Environ. Sci.*
502 *Technol.* 53 (2019) 6000-6006.
503
504 Kawakami T., Hokada T., Sakata S., Hirata T. Possible polymetamorphism and brine
505 infiltration recorded in the garnet-sillimanite gneiss, Skallevikshalsen, Lutzow-Holm
506 Complex, East Antarctica, *J. Mineral. Petrol. Sci.* 111 (2016) 129-143.
507
508 Kerper L.E., Hinkle P.M. Cellular uptake of lead is activated by depletion of
509 intracellular calcium stores, *J. Biol. Chem.* 272 (1997) 8346-8352.
510
511 Klejman M.E., Gruszczynska-Biegala J., Skibinska-Kijek A., Wisniewska M.B., Misztal
512 K., Blazejczyk M., Bojarski L., Kuznicki J. Expression of STIM1 in brain and
513 puncta-like co-localization of STIM1 and ORAI1 upon depletion of Ca²⁺ store in
514 neurons, *Neurochem. Int.* 54 (2009) 49-55.
515
516 Konz I., Fernandez B., Fernandez M.L., Pereiro R., Sanz-Medel A. Laser ablation
517 ICP-MS for quantitative biomedical applications, *Anal. Bioanal. Chem.* 403 (2012)
518 2113-2125.
519
520 Liao Y., Erxleben C., Abramowitz J., Flockerzi V., Zhu M.X., Armstrong D.L.,
521 Birnbaumer L. Functional interactions among Orai1, TRPCs, and STIM1 suggest a
522 STIM-regulated heteromeric Orai/TRPC model for SOCE/Icrac channels, *Proc. Natl.*
523 *Acad. Sci. U.S.A.* 105 (2008) 2895-2900.

524

525 Limbeck A., Galler P., Bonta M., Bauer G., Nischkauer W., Vanhaecke F. Recent
526 advances in quantitative LA-ICP-MS analysis: challenges and solutions in the life
527 sciences and environmental chemistry, *Anal. Bioanal. Chem.* 407 (2015) 6593-6617.

528

529 Mazliah J., Barron S., Bental E., Rogowski Z., Coleman R., Silbermann M. The effects
530 of long-term lead intoxication on the nervous system of the chicken, *Neurosci. Lett.* 101
531 (1989) 253–257.

532

533 Moreno-Gordaliza E., Giesen C., Lazaro A., Esteban-Fernandez D., Humanes B., Canas
534 B., Panne U., Tejedor A., Jakubowski N., Gomez-Gomez M.M. Elemental bioimaging
535 in kidney by LA-ICP-MS as a tool to study nephrotoxicity and renal protective
536 strategies in cisplatin therapies. *Anal. Chem.* 83 (2011) 7933-7940.

537

538 Nakata H., Nakayama S.M.M., Ikenaka Y., Mizukawa H., Ishii C., Yohannes Y.B.,
539 Konnai S., Darwish W.S., Ishizuka M. Metal extent in blood of livestock from Dandora
540 dumping site, Kenya: Source identification of Pb exposure by stable isotope analysis,
541 *Environ. Pollut.* 205 (2015) 8-15.

542

543 Nakata H., Nakayama S.M.M., Yabe J., Liazambi A., Mizukawa H., Darwish W.S.,
544 Ikenaka Y., Ishizuka M. Reliability of stable Pb isotopes to identify Pb sources and
545 verifying biological fractionation of Pb isotopes in goats and chickens, *Environ. Pollut.*
546 208 (2016) 395-403.

547

548 Nakayama S.M.M., Ikenaka Y., Hamada K., Muzandu K., Choongo K., Teraoka H.,
549 Mizuno N., Ishizuka M. Metal and metalloid contamination in roadside soil and wild
550 rats around a Pb-Zn mine in Kabwe, Zambia, *Environ. Pollut.* 159 (2011) 175-181.
551

552 Nakayama S.M.M., Ikenaka Y., Hamada K., Muzandu K., Choongo K., Yabe J.,
553 Umemura T., Ishizuka M. Accumulation and biological effects of metals in wild rats in
554 mining areas of Zambia, *Environ Monit Assess* 185 (2013) 4907-4918.
555

556 Nijenhuis T., Hoenderop J.G.J., Bindels R.J.M. TRPV5 and TRPV6 in Ca²⁺
557 (re)absorption: regulating Ca²⁺ entry at the gate, *Pflugers Arch.* 451 (2005) 181-192.
558

559 Noël M., Christensen J.R., Spence J., Robbins C.T. Using laser ablation inductively
560 coupled plasma mass spectrometry (LA-ICP-MS) to characterize copper, zinc and
561 mercury along grizzly bear hair providing estimate of diet. *Sci Total Environ.* 529
562 (2015) 1-9
563

564 Paul B., Hare D.J., Bishop D.P., Paton C., Nguyen V.T., Cole N., Niedwiecki M.M.,
565 Andreozzi E., Vais A., Billings J.L., Bray L., Bush A.I., McColl G., Roberts B.R.,
566 Adlard P.A., Finkelstein D.I., Hellstrom J., Hergt J.M., Woodhead J.D., Doble P.A.
567 Visualising mouse neuroanatomy and function by metal distribution using laser
568 ablation-inductively coupled plasma-mass spectrometry imaging, *Chem. Sci.* 6 (2015)
569 5383-5393.
570

571 Pozebon D., Scheffler G.L., Dressler V.L., Nunes M.A. Review of the applications of
572 laser ablation inductively coupled plasma mass spectrometry (LA-ICP-MS) to the
573 analysis of biological samples, *J. Anal. At. Spectrom.* 29 (12) (2014) 2204-2228.
574

575 Rahil-Khazen R., Bolann B.J., Myking A., Ulvik R.J. Multi-element analysis of trace
576 element levels in human autopsy tissues by using inductively coupled atomic emission
577 spectrometry technique (ICP-AES), *J Trace Elem Med Biol* 16 (2002) 15-25.
578

579 Sabolic I. Common mechanisms in nephropathy induced by toxic metals, *Nephron*
580 *Physiol* 104 (2006) 107-114.
581

582 Sedki A., Lekouch N., Gamon S., Pineau A. Toxic and essential trace metals in muscle,
583 liver and kidney of bovines from a polluted area of Morocco, *Sci. Total Environ.* 317
584 (2003) 201-205.
585

586 Shariatgorji M., Nilsson A., Bonta M., Gan J.R., Marklund N., Clausen F., Kallback P.,
587 Loden H., Limbeck A., Andren P.E. Direct imaging of elemental distributions in tissue
588 sections by laser ablation mass spectrometry, *Methods* 104 (2016) 86-92.
589

590 Skibinska-Kijek A., Wisniewska M.B., Gruszczynska-Biegala J., Methner A., Kuznicki
591 J., Immunolocalization of STIM1 in the mouse brain, *Acta Neurobiol. Exp.* 69 (2009)
592 413-428.
593

594 Smith R.M., Griel L.C., Muller L.D., Leach R.M., Baker D.E. Effects of dietary
595 cadmium chloride throughout gestation on blood and tissue metabolites of primigravid
596 and neonatal dairy cattle, *J. Anim. Sci.* 69 (1991) 4078-4087.
597

598 Takano T., Okutomi Y., Mochizuki M., Ochiai Y., Yamada F., Mori M., Ueda F.
599 Biological index of environmental lead pollution: accumulation of lead in liver and
600 kidney in mice, *Environ Monit Assess* 187 (2015) 1-5.
601

602 Urgast D.S., Ou O., Gordon M.J., Raab A., Nixon G.F., Kwun I.S., Beattie J.H.,
603 Feldmann J. Microanalytical isotope ratio measurements and elemental mapping using
604 laser ablation ICP-MS for tissue thin sections: zinc tracer studies in rats, *Anal. Bioanal.*
605 *Chem.* 402 (2012) 287-297.
606

607 Vassanelli S., Fromherz P. Transistor records of excitable neurons from rat brain, *Appl*
608 *Phys A Mater Sci Process* 66 (1998) 459-463.
609

610 Wang L., Chen D.W., Wang H., Liu Z.P. Effects of lead and/or cadmium on the
611 expression of metallothionein in the kidney of rats, *Biol Trace Elem Res* 129 (2009)
612 190-199.
613

614 Wang L.M., Becker J.S., Wu Q., O M.F., Bliveira M.F., Bozza F.A., Schwager A.L.,
615 Hoffman J.M., Morton K.A. Bioimaging of copper alterations in the aging mouse brain
616 by autoradiography, laser ablation inductively coupled plasma mass spectrometry and
617 immunohistochemistry. *Metallomics.* 2 (2010) 348-353.

618

619 Wlostowski T., Bonda E., Krasowska A. Free-ranging European bisons accumulate
620 more cadmium in the liver and kidneys than domestic cattle in north-eastern Poland, *Sci.*
621 *Total Environ.* 364 (2006) 295-300.

622

623 Wu B., Zoriy M., Chen Y., Becker J.S. Imaging of nutrient elements in the leaves of
624 *Elsholtzia splendens* by laser ablation inductively coupled plasma mass spectrometry
625 (LA-ICP-MS), *Talanta.* 78 (2009) 132-137.

626

627 Yabe J., Nakayama S.M.M., Ikenaka Y., Muzandu K., Choongo K., Mainda G., Kabeta
628 M., Ishizuka M., Umemura T. Metal distribution in tissues of free-range chickens near a
629 lead-zinc mine in Kabwe, Zambia, *Environ. Toxicol. Chem.* 32 (2013) 189-192.

630

631 Yabe J., Nakayama S.M.M., Ikenaka Y., Muzandu K., Ishizuka M., Umemura T.
632 Accumulation of metals in the liver and kidneys of cattle from agricultural areas in
633 Lusaka, Zambia, *J. Vet. Med. Sci.* 74 (2012) 1345-1347.

634

635 Yamashita S., Yoshikuni Y., Obayashi H., Suzuki T., Green D., Hirata T. Simultaneous
636 Determination of Size and Position of Silver and Gold Nanoparticles in Onion Cells
637 using Laser Ablation-ICP-MS. *Anal. Chem.* 91. (2019) 4544-4551.

638

639 Zhang H., Li W., Xue Y., Zou F. TRPC1 is involved in Ca²⁺ influx and cytotoxicity
640 following Pb²⁺ exposure in human embryonic kidney cells, *Toxicol. Lett.* 229 (2014)
641 52-58.

Table 1. Mean \pm SD of the Pb concentration in the blood and organs of mice for the three dosage groups.

| | Control | Low | High |
|----------------------------|---------------------|--------------------|---------------------|
| Blood ($\mu\text{g/dL}$) | 1.8 ± 0.5^a | 14.9 ± 3.2^b | 40.8 ± 3.9^c |
| Liver (mg/kg) | 0.016 ± 0.001^a | 4.54 ± 0.59^b | 16.49 ± 1.58^c |
| Kidney (mg/kg) | 0.044 ± 0.002^a | 11.47 ± 1.48^a | 56.65 ± 20.20^b |
| Brain (mg/kg) | 0.027 ± 0.008^a | 0.54 ± 0.09^b | 2.66 ± 0.33^c |

Note:

Different letters (a, b, and c) between columns indicate a significant difference between dosage groups ($p < 0.05$).

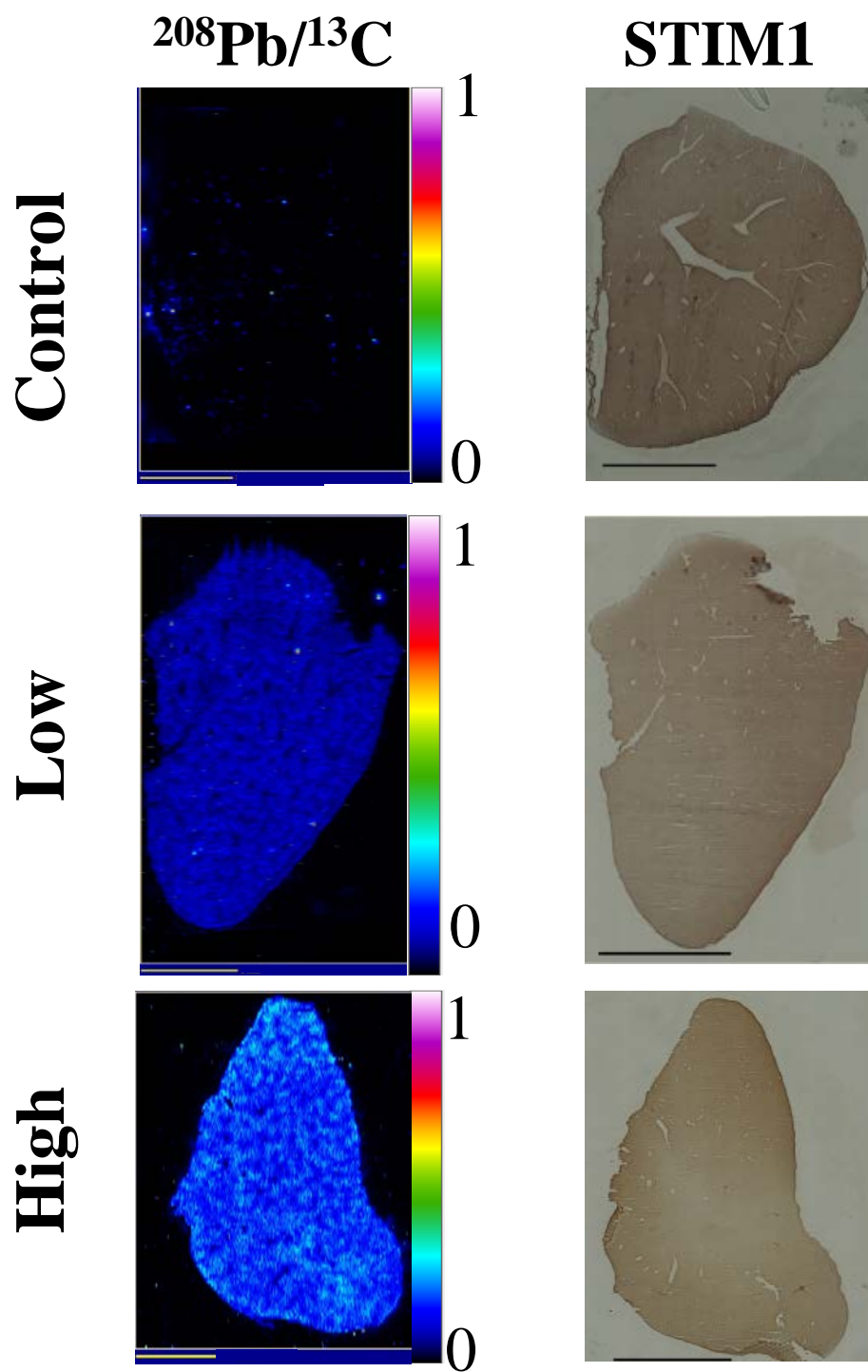


Figure 1.

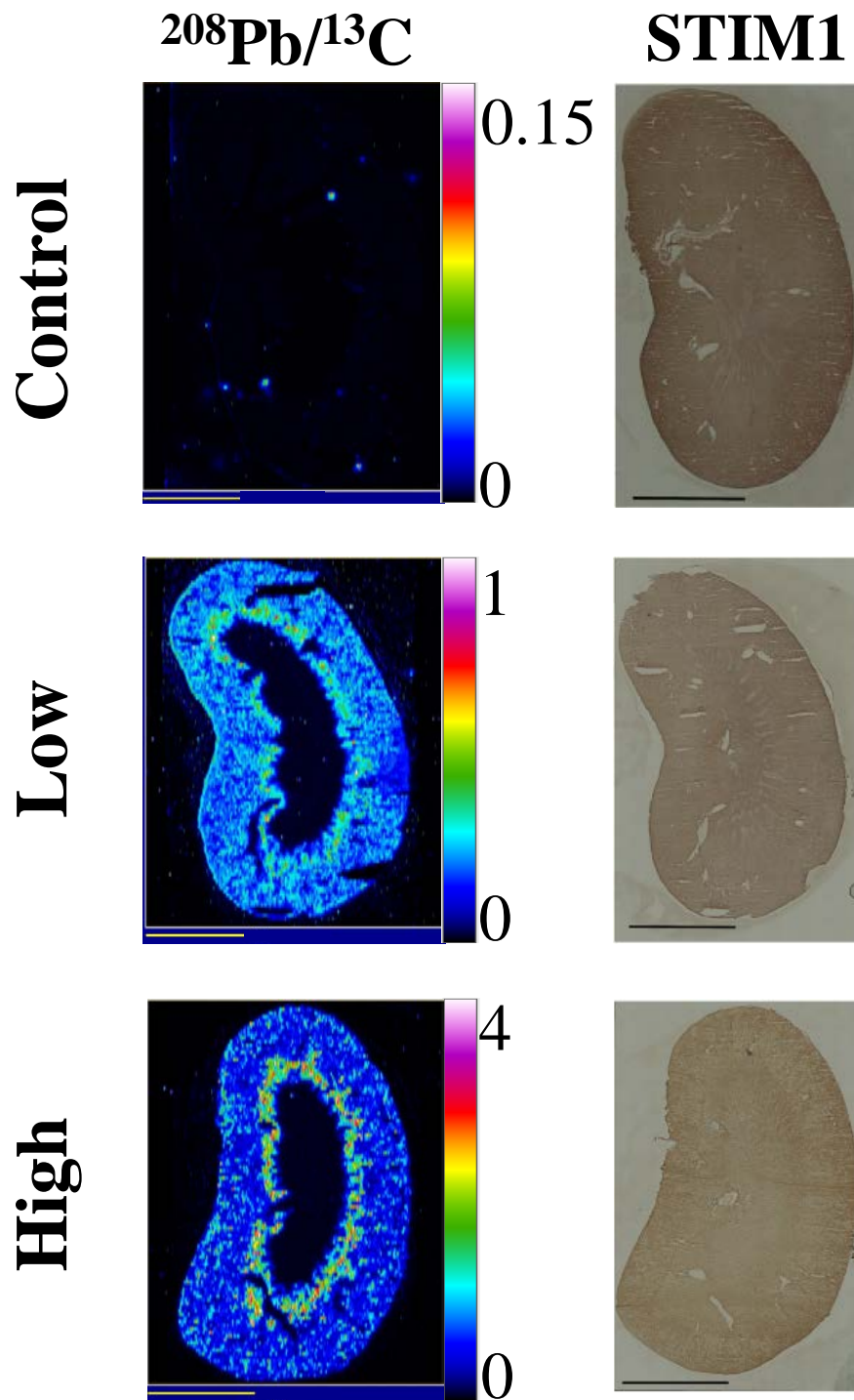


Figure 2.

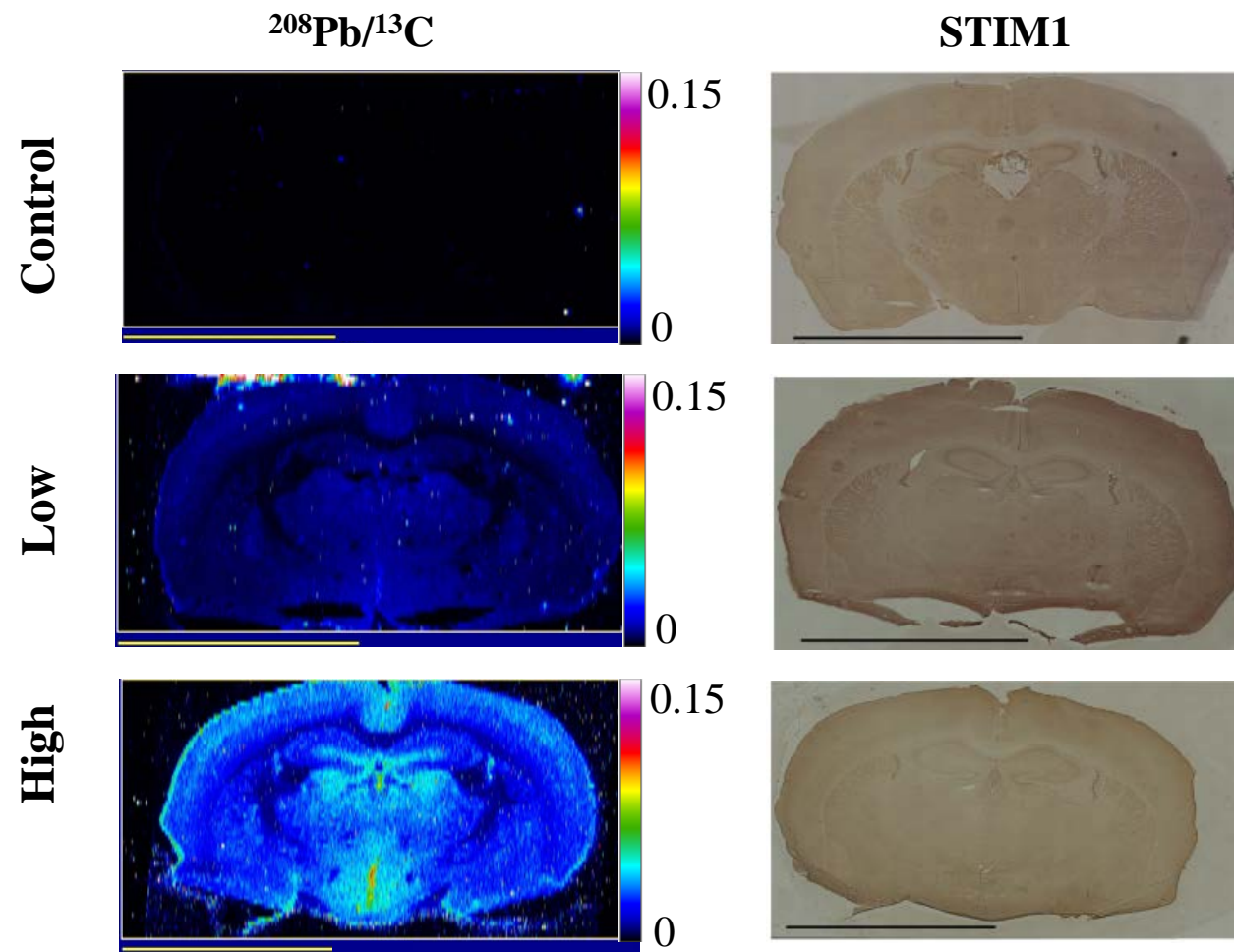


Figure 3.

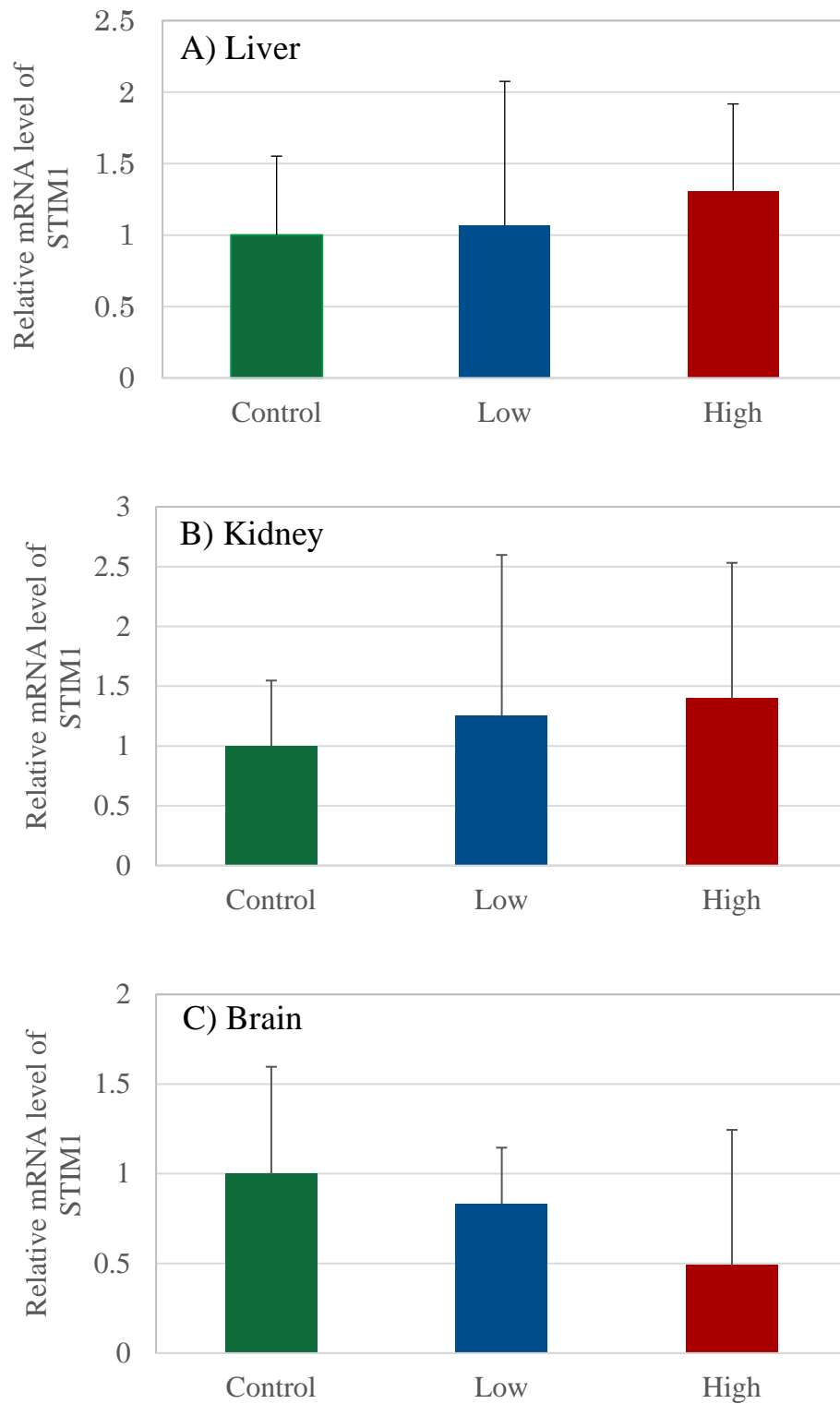


Figure 4.